Optimizing the Ultrawide-Band Photonic Link

Lee T. Nichols, Keith J. Williams, and Ronald D. Esman, *Senior Member, IEEE*

***Abstract*— Performance of wide-band photonic links (PL's) using Mach–Zehnder modulators (MZM's) is reported. Comparison parameters include loss, noise figure, and spur-free dynamic range (SFDR). The feasibility of a 0-dB noise-figure link even with passive matching is given and the advantages of dual-output MZM's are presented. A new figure of merit is introduced to quantitatively optimize link performance with or without a preamplifier.**

***Index Terms*—Cascade systems, impedance matching, intensity modulation, intermodulation distortion, optical fiber delay lines, sensitivity.**

I. Introduction

As THE USE OF photonic links (PL's) increases in wide-band microwave systems, the capabilities of such links in terms of sensitivity and dynamic range become critical. Existing assessments of link performance [1]–[3] do not sufficiently address the effects of broader bandwidths, higher photocurrents, lower relative intensity noise (RIN), modulator half-wave voltage, and external preamplifiers. In this paper, we expand the basic model presented heretofore to account for multioctave and balanced-detection PL's. This model, combined with clear performance goals, highlights key design parameters in the PL as well as in the accompanying microwave components. By introducing a simple figure of merit which integrates sensitivity and dynamic range and applying it to cascaded systems, we quantify the tradeoffs which arise when the PL is interfaced with a microwave system. We also clarify the notion [1], [3], [4] that microwave PL's are fundamentally limited to noise figures >3 dB by input matching considerations.

In order to establish a baseline, we focus on unconditioned PL's as opposed to links involving linearization schemes [5], [6]. Since state-of-the-art dynamic ranges are currently achieved using externally-modulated links, we consider these rather than direct modulation techniques. To simplify further, we look only at intensity-modulated direct-detection (IMDD) links where the output photocurrent is the baseband signal. Indirect alternatives are summarized in [7].

II. Link Noise

Noise power in IMDD links is typically dominated by three effects: thermal, shot, and intensity noise. Output thermal noise power comprises that created at the output of the link $N_{tR} = k_BTB$ and that created at the input to the active portion and amplified by subsequent link gain $N_{tT} = k_BTBG/k_{\rm in}$; where k_B is Boltzmann's constant, T is temperature, B is the receiver bandwidth, G is the RF gain of the entire PL, and $k_{\rm in}$ accounts for passive impedance matching to the modulator RF input. Shot and intensity noise depend on detected optical power, detection scheme, and photodetector (PD) impedance matching. The outputs of dual-output (X-coupled) Mach–Zehnder modulators (MZM's) carry the same IM signal 180° out of phase allowing a balanced-detection scheme [8]. The photocurrents for the single-output (Y-coupled) MZM and for each arm of the X-coupled MZM are

$$\begin{aligned} i_Y &= i\{1+\cos[\Delta\phi_Y+\phi_m(t)]\} \\ i_{X\pm} &= \frac{1}{2}i\{1\pm\cos[\Delta\phi_X+\phi_m(t)]\} \end{aligned} \tag{1}$$

where i is the total dc photocurrent at quadrature, $\Delta\phi_Y$ is the static phase shift between arms, $\phi_m(t)$ is the modulated phase, and $\Delta\phi_X \equiv \Delta\phi_Y - \pi/2$ yields a similar functional form in the balanced coupler case. Although PD nonlinearities are typically present above ~ 1 mA of photocurrent [9], for this paper we exclude these effects.

The output shot noise power [10] is proportional to the total photocurrent

$$N_{sY} \approx 2k_{\rm out}eiR_lB(1+\cos\Delta\phi), \qquad N_{sX} = 2k_{\rm out}eiR_lB \tag{2}$$

where e is electronic charge, R_1 is the system load (or source) impedance, and $k_{\rm out}$ is an output impedance-match correction. The correlated-intensity noise power from each PD of the balanced detector coherently subtracts, assuming path lengths from modulator to detector and PD amplitude responses are well matched. Therefore, the intensity noise power [11] is given by

$$\begin{aligned} N_{iY} &\approx k_{\rm out}i^2R_lt_iB(1+\cos\Delta\phi)^2 \\ N_{iX} &\approx \frac{1}{2}k_{\rm out}i^2R_lt_iB(1+\cos 2\Delta\phi) \end{aligned} \tag{3}$$

where t_i is the RIN. The approximation symbols used in the above expressions indicate that the small-signal approximation is being used.

III. Gain, Noise Figure, and Linearity

To quantify these parameters, we assume $\phi_m = \phi(\cos\omega_1 t + \cos\omega_2 t)$ where $\phi = \pi\sqrt{2k_{\rm in}R_lP}/v_\pi$, P is the input RF power to the MZM, and v_π is the half-wave voltage. Noting that the photocurrent in the balanced detector configuration is the difference of $i_{X\pm}$ in (1), we evaluate the photocurrent using

Manuscript received December 5, 1996; revised April 24, 1997. This work was supported by the Office of Naval Research Accelerated Capabilities Initiative.

The authors are with the Naval Research Laboratory, Washington, DC 20375-5338 USA.

Publisher Item Identifier S 0018-9480(97)05984-X.

Bessel functions [12] shown in (4) at the bottom of this page, where only sum terms are used for harmonics. Noting that the performance of the X-coupled PL should be compared to that of the Y-coupled PL at half the current (same optical source power), the small-signal RF gain can be written using the same expression for both coupling configurations as follows:

$$G = k_{\text{in}} k_{\text{out}} (\pi i R_l \sin \Delta\phi / v_\pi)^2. \tag{5}$$

For low v_π (high gain), thermal noise at the MZM · RF input contributes significantly to output noise which, for a passively-matched input, is thereby independent of k_{in}. For active matching, thermal noise at the input to the matching network must also be considered.

Since noise figure is defined [13] as

$$F \equiv \text{total output noise}/Gk_BTB = N/Gk_BTB \tag{6}$$

the PL noise figure approaches 0 dB if the modulator input is impedance matched with negligible loss and $N_{tT} \gg N_{tR} + N_s + N_i$. But practically, as shown in Fig. 1, RIN limits the sensitivity which can be obtained [14]. (In all figures, the following are assumed unless otherwise indicated: $k_{\text{out}} = 1$, $t_i = 0.1$ fs (-160 dB/Hz), $R_l = 50\,\Omega$, $T = 300$ K). Note that the noise figure of a quadrature-biased Y-coupled PL with a -170 dB/Hz RIN source and 10-mA photocurrent can actually be improved by 4 dB using balanced detection. Also, the X-coupled link data in Fig. 1 and the remainder of this paper assumes ideal RIN cancellation as in (3). In a practical sense, balanced detection offers at least 20 dB of suppression: at high i, the performance indicated by a particular Y-coupled curve in Fig. 1 can be achieved by an X-coupled PL using an optical source with roughly 20 dB greater RIN.

It has been asserted [4] that, for a "lossless passive matching" network, the modulator-input matching resistor contributes an additional k_BTB to N_{tT} such that the fundamental noise figure limit is 3 dB. In contrast, we consider such a resistor to be integral to the matching network which, therefore, is lossy, gives $k_{\text{in}}<1$, and from $N_{tT} = k_BTBG/k_{\text{in}}$ results in a > 0 dB noise-figure limit. Note that for a traveling-wave modulator at traveling-wave frequencies, the noise generated by a matching resistor (at the RF output of the modulator electrodes) is counterpropagating to the optical wave. Hence, its modulation efficiency is severely reduced, leading to $<$ 3-dB noise figure. Also in principle, a modulator can be designed to deliver RF input power to an antenna so that no terminating resistor is needed, and again, the noise figure would be $<$ 3 dB. In addition, we point out that impedance mismatch may be traded off for ultralow noise figure in some cases.

In a multioctave bandwidth, either second- or third-order intercept powers (IP's) can become the limiting distortion terms

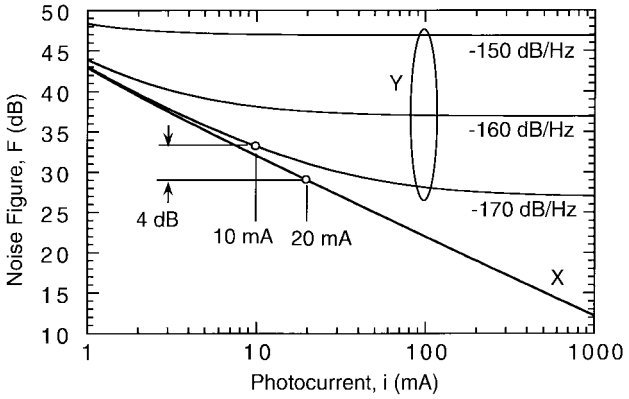

Fig. 1. Noise figure comparison of quadrature-biased X- and Y-coupled IMDD PL's for optical sources with varying RIN. Assumptions: $k_{\text{in}} = 1$ and $v_\pi = 10$ V.

depending upon MZM bias. Using small-signal approximations in (4), the output second- and third-order intermodulation IP's (OIP2 and OIP3) are [15]

$$\begin{aligned} P^{(2)} &\approx 2k_{\text{out}} i^2 R_l \sin^2 \Delta\phi \tan^2 \Delta\phi \\ P^{(3)} &\approx 4k_{\text{out}} i^2 R_l \sin^2 \Delta\phi. \end{aligned} \tag{7}$$

This and other previous expressions are fairly well known and serve as background for the remainder of this paper.

IV. Spur-Free Dynamic Range and Performance Comparisons of Alternative PL Configurations

Combining small-signal output noise power and intercept values, we have

$$\begin{aligned} R_Y &\approx \min\left[\left(\frac{P^{(3)}}{N_Y}\right)^{2/3}, \sqrt{\frac{P^{(2)}}{N_Y}}\right] \\ R_X &\approx \min\left[\left(\frac{P^{(3)}}{N_X}\right)^{2/3}, \sqrt{\frac{P^{(2)}}{N_X}}\right] \\ N_Y &\equiv N_{tR} + N_{tT} + N_{sY} + N_{iY} \\ N_X &\equiv N_{tR} + N_{tT} + N_{sX} + N_{iX} \end{aligned} \tag{8}$$

where R is the spur-free dynamic range (SFDR). While the single-octave R_Y is well known [5], the multioctave expressions extend the model to include second-order distortion contributions from all even-order terms of the link transfer function Taylor expansion. Indeed, a more complete nonlinear model is expressed by $R \approx \min[(P^{(n)}/N)^{[(n-1)/n]}]$ [6] where n is the distortion product order. The expressions for R_X further extend the model to balanced PL's. Fig. 2 illustrates (8) versus bias for PL's with the same optical source power. An additional curve shows the relative insensitivity of the

$$\begin{aligned} i_Y &= i + i_X \\ i_X &= i \times \begin{cases} J_0^2(\phi)\cos\Delta\phi & m = n = 0 \\ 2(-1)^{\frac{m+n}{2}} J_m(\phi) J_n(\phi) \cos\Delta\phi \cos(m\omega_1 \pm n\omega_2)t & m+n \text{ even} \\ 2(-1)^{\frac{m+n+1}{2}} J_m(\phi) J_n(\phi) \sin\Delta\phi \cos(m\omega_1 \pm n\omega_2)t & m+n \text{ odd} \end{cases} \end{aligned} \tag{4}$$

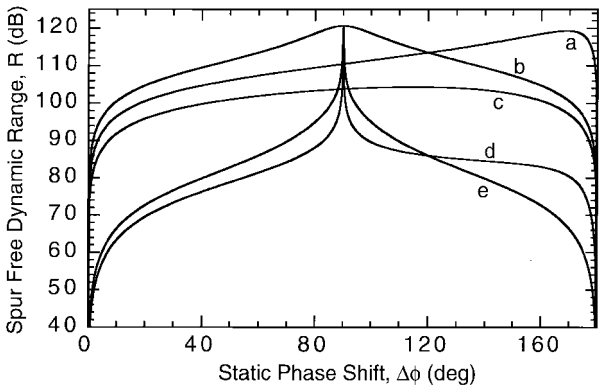

Fig. 2. SFDR comparison of IP2- and IP3-limited X- and Y-coupled IMDD PL's. Assumptions: $v_\pi = 10$ V and $B = 1$ Hz. a: 50 mA, Y, single-octave, b: 100 mA, X, single-octave, c: 0.5 mA, Y, single-octave, d: 50 mA, Y, multioctave, e: 100 mA, X, multioctave.

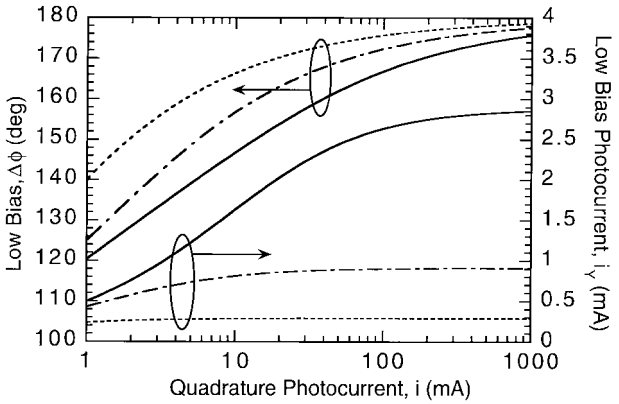

Fig. 3. Optimum phase bias and resulting photocurrent as a function of quadrature photocurrent for Y-coupled single-octave IMDD PL's with RIN as indicated: ——: −170 dB/Hz; —•—•—: −160 dB/Hz; – – –: −150 dB/Hz.

standard low-current single-octave PL to MZM bias. As bias is varied, more or less optical power is transmitted changing both N and $P^{(n)}$. Note that, in a multioctave system, the SFDR is described by the IP2-related value except near quadrature, where the limiting value is IP3-related.

There are a number of conclusions to be drawn regarding unconditioned PL's from (8). First, in a balanced-detection system, the optimum bias is quadrature. As B increases and the SFDR is reduced, the relative separation between the IP3- and IP2-related curves decreases somewhat so that the range of acceptable bias points near quadrature widens. Second, the multioctave single-output link SFDR (also optimized at quadrature) has an upper limit with increasing photocurrent approximated by a simple expression: $R_Y|_{\pi/2} \approx (4/Bt_i)^{2/3}$. Third, in a single-octave single-output IMDD link, optimum bias approaches 180° with increasing photocurrent; this is the "low-biasing" method [2]. The optimum bias is found analytically to satisfy the following relation:

$$1+\cos\Delta\phi = \left[\sqrt{b^2+4bei+4bt_ii^2}-b\right]/(2ei+2t_ii^2) \qquad (9)$$

where $b \equiv k_BT/k_{\text{out}}R_l$. This relation and the photocurrent at optimum low bias are pictured for various RIN in Fig. 3. Note that, for increasing t_i, the photocurrent must be clamped at lower values to retain thermal- or shot-limited noise, comparable to that of the balanced PL.

Since the OIP3 expression is the same for both X- and Y-coupled configurations, the low-biased single-octave PL SFDR will be comparable to that of the balanced PL as shown in Fig. 4 along with the RIN-limited quadrature-biased Y-coupled PL. However, there are practical disadvantages with low-biasing. First, unlike a balanced PL, the low-biased PL does not offer shot-noise limited SFDR in a multioctave system. Second, low-biased links suffer increased link loss relative to balanced-detection PL's according to (5). As shown in Fig. 5, the gain increase due to higher optical source power is partially undercut by MZM transmission loss in the low-biased link. Again, the SFDR or gain of the balanced-detection PL should be compared to that of the Y-coupled PL at half the current: increasing photocurrent from 1 to 100 mA in the balanced-detection scheme reduces the loss by 40 dB, whereas

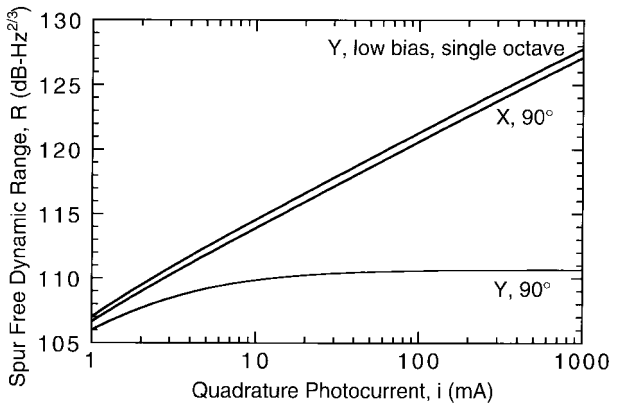

Fig. 4. SFDR comparison of quadrature-and low-biased X- and Y-coupled IMDD PL's. For the low-bias case, quadrature photocurrent refers to the photocurrent prior to applying the appropriate low bias. Assumption: $v_\pi = 10$ V.

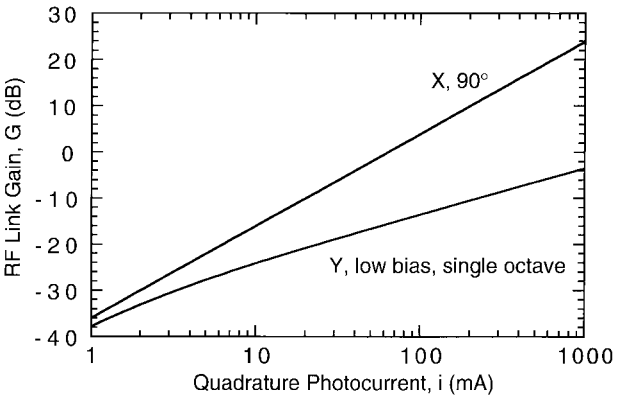

Fig. 5. RF link gain comparison of balanced detection and low-biased IMDD PL's. Assumptions: $k_{\text{in}} = 1$ and $v_\pi = 10$ V.

increasing it from 0.5 to 50 mA in the low-biasing scheme results in only a 26.3-dB improvement. Thus, at high i, the Y-configured link requires more preamplifier gain to achieve given net link gain and, thereby, risks SFDR reduction. Also, low-biased link RF gain decreases with increasing t_i due to (9), degrading its sensitivity.

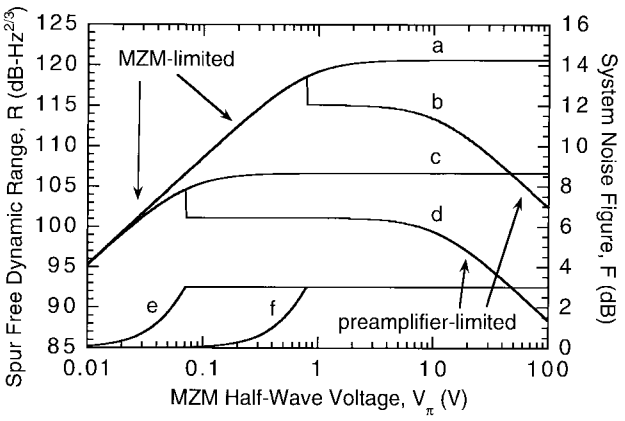

Fig. 6. SFDR comparison of X-coupled quadrature-biased IMDD PL's designed to meet a maximum 3-dB noise-figure specification using a typical preamplifier where necessary. Assumptions: $k_{\rm in} = 1$, OIP3$_{\rm amp} = 30$ dBm, and $F_{\rm amp} = 2.3$ dB. a: SFDR, 100 mA, no preamplifier, b: SFDR, 100 mA, preamplified, c: SFDR, 1 mA, no preamplifier, d: SFDR, 1 mA, preamplified, e: noise figure, 1 mA, preamplified, f: noise figure, 100 mA, preamplified.

A third disadvantage of the low-biased PL is that SFDR, link gain, and transmitted photocurrent are very sensitive functions of MZM bias. As shown in Fig. 2, at 50 mA, the bias approaches the transmission null of the MZM. On the side of the peak facing away from the null, a 10° error reduces SFDR by 0.9 dB. But on the null side, the same error reduces SFDR by 10.1 dB. The same errors in the 100-mA balanced link reduce SFDR by only 2 dB. A $\pm$ 5° error in the 100-mA quadrature X-coupled PL leads to gain variation of 0.033 dB with constant total photocurrent. In contrast, the same error in the low-biased link at 50 mA causes the gain to vary by 8.6 dB and the photocurrent to vary by a factor of 7.4, making the link orders of magnitude more sensitive to bias drift or thermal noise at the bias input to the MZM and, in the worst case, risking PD failure due to high current. Finally, recalling that i_Y differs from its small-signal value when the MZM is off quadrature, it is apparent that the low-biased link will generally have more noise, less dynamic range, and less RF link gain than indicated by Figs. 4–6. This is particularly true for high i PL's because the bias is so close to the null that the small-signal approximation conditions [used for (2), (3), (5), (7), and (8)] are never met. For these reasons, we conclude that the balanced configuration PL makes better use of optical source power and, therefore, we will limit subsequent discussion to these links.

V. Optimizing the Photonic Link

It has been shown [1] that reduced v_π can eventually reduce PL SFDR. Sensitivity requirements sometimes necessitate this penalty in favor of lower noise figure. Similarly when choosing preamplifiers with the same noise figure and OIP3, but differing RF gain, (6) and (8) imply that the higher gain amplifiers will necessarily have lower SFDR. Improved PL sensitivity requires less preamplifier gain to achieve overall sensitivity and can, therefore, improve overall dynamic range. To quantify these tradeoffs, we consider three scenarios: minimum specified SFDR, maximum specified noise figure, and simultaneously optimized SFDR and noise figure. For simplicity, we also consider only single-octave systems.

For two-port devices, the dynamic range of a cascade is never greater than that of the lowest dynamic range component provided the output noise of all components except the last is much greater than thermal noise. This is easily seen if (8) is computed using the noise-figure equation [13] and the expression for cascading distortion OIP's [15]

$$N_{12} = N_2 + G_2(N_1 - k_B T B)$$
$$\frac{1}{P_{12}^{(3)}} = \frac{1}{G_2 P_1^{(3)}} + \frac{1}{P_2^{(3)}}. \tag{10}$$

Since the PL is essential, one tries to meet the specifications first by optimizing the PL and then by including a preamplifier if necessary. Note that *conditioned* links involve a linearization scheme which invalidates the second expression in (10) because of nonzero phase between distortion products in each component, eliminating the constraint on net SFDR. Distortion cancellation can be taken into account [5], [15] and the *conditioned* PL treated as a single component with set values of G, F, and P, in which case the following analysis regarding preamplifier selection is still valid.

A. Minimum SFDR Specified

We assume a technological limitation $i_{\rm max}$ because, as we have seen, R, F, and G improve with increased i. The maximum SFDR requirement which can be met by the PL (and, therefore, the cascaded system) is given by (8) with $i = i_{\rm max}$ and $v_\pi \to \infty$. It may seem odd that maximum SFDR is obtained for a modulator with maximum conversion loss, but this is simply because such a device can handle more input power without distortion. If the SFDR requirement is less than this maximum value, then the optimum value of v_π is the least value which will meet the requirement because this value will produce the lowest noise figure. Preamplifiers need not be discussed due to the "bottleneck" described above: if the SFDR requirement is not met, there is no way to meet it using another device; if it is met, adding a preamplifier reduces the SFDR. One might argue that reducing R could be traded for lowering F; however, this means SFDR is not really a hard requirement and the third scenario below is better suited to solving the problem.

B. Maximum Noise Figure Specified

In the second scenario, we divide possible values of v_π into two regions: the low values satisfying a minimum F requirement and the high values which necessitate a preamplifier to meet it. If minimum preamp gain $G_{\rm min}$ is used in the latter case, the output noise is independent of $G_{\rm min}$ and depends on PL gain only to the extent that $k_{\rm in}$ departs from unity

$$N_{12} = \frac{F_{12}}{F_{12} - F_1}\left\{N_s + N_i + k_B T B\left[1 + \frac{G_2}{k_{\rm in}}(1 - k_{\rm in})\right]\right\}. \tag{11}$$

As a result, for nearly-lossless input impedance matching, R has the same logarithmic dependence on v_π as the cascaded

OIP3. This is demonstrated in Fig. 6 where $<$ 3-dB noise figure is specified. The discontinuity represents the boundary between the two v_π regions. To satisfy the requirement with increasing v_π, larger preamplifier gain is required reducing preamplifier SFDR and, thereby, system SFDR. The SFDR will be optimized for the largest value of v_π where the noise-figure requirement is met by the PL alone.

C. Optimizing Both Noise Figure and SFDR

In the third scenario, we resolve the tradeoff between dynamic range and sensitivity directly by defining a figure of merit: $M \equiv R/F$. The dependence of this quantity on all link parameters except v_π follows that of SFDR. For example, since R increases and F decreases with increasing i, M will also increase. One can also show that the optimum bias values are as previously stated using the following arguments. In the dual-octave case, the tangent dependence in (7) of the OIP2 dominates so that the optimum bias is quadrature. In the single octave case, $1/F$ and $R^{3/2}$ have the same functional dependence on $\Delta\phi$ because $P^{(3)}$ and G have the same functional dependence on $\sin^2\Delta\phi$. As a result, the balanced configuration is optimized at quadrature as before and the optimum bias in the Y-coupled configuration is again described by (9).

The utility of the figure of merit becomes apparent when we compute the optimum value of v_π. Since v_π only enters (8) through the quantity G, we can answer this question by setting the derivative of M with respect to G equal to zero as follows:

$$G\big|^{(3)}_{\partial M/\partial G=0} = \frac{3}{2}[1+(N_s+N_i)/k_BTB]. \qquad (12)$$

In other words, increasing gain (decreasing v_π) above the value where $N_{tT} \approx N_{tR}+N_s+N_i$ reduces M by decreasing R, while decreasing G below this value reduces M by decreasing sensitivity. The additional factor of 3/2 is a consequence of the distortion order considered. For second-order dominated SFDR, this factor is 2; for SFDR dominated by nth-order distortion products, the factor is $n/(n-1)$. Having determined the optimum v_π, we can also use the merit to help us select a preamplifier. That is, the optimum preamp gain G_1, assuming the preamplifiers have the same noise figure F_1 and OIP3 $P_1^{(3)}$, is given by

$$G_1\big|^{(3)}_{\partial M/\partial G_1=0} = \frac{3}{2}[(F_2-1)/F_1]. \qquad (13)$$

This relation shows that the merit is optimized when the contributions of the preamp and PL noise figures to the cascaded-system noise figure are roughly equal. To illustrate results (12) and (13), we show M in Fig. 7 for X-coupled IMDD PL's at different currents as well as M obtained using a preamp selected according to (13). The peaks of the two curves representing PL's alone occur at v_π values given by (12). Note that from (6), the noise figure at these peaks is $(2/3)+(1/k_{\rm in})$ or for nearly lossless impedance matching, 2.22 dB. The peak SFDR values MF approach those shown in Fig. 6 for PL's with the same parameters. These results demonstrate that the figure of merit is a quantitative guide toward systems which have useful sensitivity and dynamic range near the obtainable maxima $(v_\pi \to \infty)$.

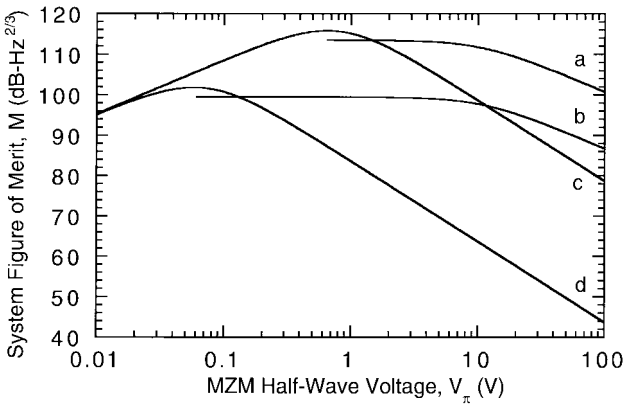

Fig. 7. Figure of merit comparison of X-coupled quadrature-biased IMDD PL's with and without preamplifiers. Assumptions: $k_{\rm in} = 1$, OIP3$_{\rm amp}$ = 30dBm, and $F_{\rm amp} = 2.3$ dB. a: 100 mA, preamplified, b: 1 mA, preamplified, c: 100 mA, no preamplifier, d: 1 mA, no preamplifier.

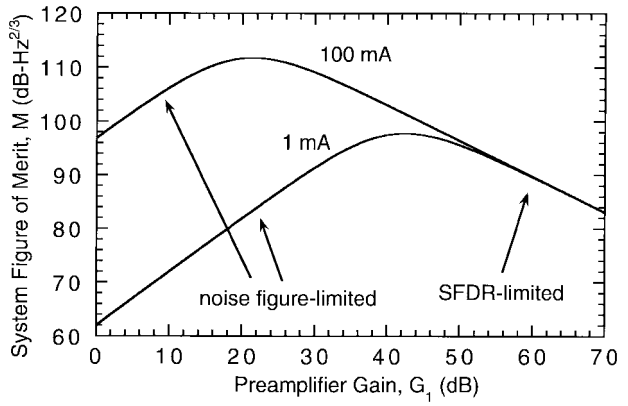

Fig. 8. Figure-of-merit comparison of preamplified X-coupled quadrature-biased IMDD PL's with varying preamplifier gain. Assumptions: $k_{\rm in=1}$, $v_\pi = 10$ V, OIP3$_{\rm amp}$ = 30 dBm, and $F_{\rm amp} = 2.3$ dB.

Considering now the effect of the preamplifier, it can be shown by calculating the PL gain G_2 at optimum v_π and inserting this value into the second expression of (10), that the OIP3 of the cascade does not significantly increase with increased preamplifier output power. Therefore, the cascade figure of merit M_{12} is also limited by a "bottleneck effect": it can never be greater than that of the PL itself at its optimum v_π. Nevertheless, for links constrained to a minimum half-wave voltage $v_{\pi,\rm min}$ greater than the optimum value, the figures of merit shown in Fig. 7 for preamplified PL's clearly indicate that the advantage of reduced noise figure can outweigh the disadvantage of reduced SFDR provided the preamplifiers are carefully selected. The need for careful selection is demonstrated in Fig. 8, where the figures of merit for preamplified PL's with varying G_1 are shown at $v_{\pi,\rm min} =$ 10 V. By using (10) and (13), the cascade noise figure at the peaks (and along the preamplified link curves in Fig. 7) is given by $F_{12} = 5F_1/3$, only 2.22 dB greater than that of the preamplifier. The figure of merit can be modified to suit the priorities of the link designer. One can favor R or F using a more general definition: $M = R^m/F^n$. This would shift

optimum values slightly in the direction which improves the favored parameter and alter the slopes of the asymptotes on either side of the peaks by the appropriate factor m or n.

VI. Conclusion

Photonic-link performance has been revisited and expanded. The passive input matching constraint on lowest achievable PL noise figure has been clarified. Quantitative results have been derived comparing single- and multioctave bandwidth low-biased and balanced configuration link performance and an exact relation for the low-biasing scheme has been presented. These comparisons reveal that low-biased PL performance is generally inferior to that of the balanced PL. Also, new insight into the problem of optimizing this performance over key design parameters of the PL itself and of an accompanying microwave preamplifier has been provided using a new figure of merit which simultaneously accounts for changes in noise figure and SFDR, allowing for quantitative analysis of the resulting tradeoffs.

Acknowledgment

The authors would like to thank Dr. M. Frankel for helpful comments on matching network issues.

References

[1] E. Ackerman, S. Wanuga, D. Kasemset, A. S. Daryoush, and N. R. Samant, "Maximum dynamic range operation of a microwave external modulation fiber-optic link," *IEEE Trans. Microwave Theory Tech.*, vol. 41, pp. 1299–1306, Aug. 1993.

[2] M. L. Farwell, W. S. C. Chang, and D. R. Huber, "Increased linear dynamic range by low biasing the Mach–Zehnder modulator," *IEEE Photon. Technol. Lett.*, vol. 5, pp. 779–782, July 1993.

[3] C. H. Cox III, G. E. Betts, and L. M. Johnson, "An analytic and experimental comparison of direct and external modulation in analog fiber-optic links," *IEEE Trans. Microwave Theory Tech.*, vol. 38, pp. 501–509, May 1990.

[4] C. H. Cox III, E. I. Ackerman, and G. E. Betts, "Relationship between gain and noise figure of an optical analog link," in *MTT-S Symp. Dig.*, San Francisco, CA, June 1996, pp. 1551–1554.

[5] G. E. Betts, "Linearized modulator for suboctave-bandpass optical analog links," *IEEE Trans. Microwave Theory Tech.*, vol. 42, pp. 2642–2649, Dec. 1994.

[6] J. H. Schaffner and W. B. Bridges, "Intermodulation distortion in high dynamic range microwave fiber-optic links with linearized modulators," *J. Lightwave Technol.*, vol. 11, pp. 3–6, Jan. 1993.

[7] R. F. Kalman, J. C. Fan, and L. G. Kazovsky, "Dynamic range of coherent analog optical fiber-optic links," *J. Lightwave Technol.*, vol. 12, pp. 1263–1277, July 1994.

[8] E. I. Ackerman, S. Wanuga, J. MacDonald, and J. Prince, "Balanced receiver external modulation fiber-optic link architecture with reduced noise figure," in *MTT-S Symp. Dig.*, Atlanta, GA, June 1993, pp. 723–726.

[9] K. J. Williams, R. D. Esman, and M. Dagenais, "Nonlinearities in p-i-n microwave photodetectors," *J. Lightwave Technol.*, vol. 14, pp. 84–96, Jan. 1996.

[10] A. Yariv, *Optical Electronics*. Philadelphia, PA: Saunders, 1991, pp. 364–372.

[11] G. L. Abbas, V. W. S. Chan, and T. K. Yee, "A dual-detector optical heterodyne receiver for local oscillator noise suppression," *J. Lightwave Technol.*, vol. LT-3, pp. 1110–1122, Oct. 1985.

[12] B. H. Kolner and D. W. Dolfi, "Intermodulation distortion and compression in an integrated electrooptic modulator," *Appl. Opt.*, vol. 26, no. 17, pp. 3676–3680, Sept. 1987.

[13] K. Chang, *Microwave Solid-State Circuits and Applications*. New York: Wiley, 1994, p. 185.

[14] K. J. Williams and R. D. Esman, "Optically amplified downconverting link with shot-noise-limited performance," *IEEE Photon. Technol. Lett.*, vol. 8, pp. 148–150, Jan. 1996.

[15] S. A. Maas, *Nonlinear Microwave Circuits*. New York: McGraw-Hill, 1995, pp. 155–207.

Lee T. Nichols received the B.A. degree (with high honors) from the University of Texas at Austin, in 1992, and the M.S. degree in electrical engineering from the University of Colorado, Boulder, in 1994.

In 1995, he joined the Naval Research Laboratory, Washington, DC, where he presently works in the Microwave Photonics Section, developing fiber-optic systems for antenna remoting and signal processing.

Mr. Nichols is a member of Phi Beta Kappa.

Keith J. Williams was born in Lincoln, NE, on March 17, 1964. He received the B.S. degree (*cum laude*) in electrical engineering from the University of Nebraska, Lincoln, in 1987, and the M.S. and Ph.D. degrees in electrical engineering from the University of Maryland at College Park, in 1989 and 1994, respectively.

In 1987, he joined the Optical Techniques Branch of the Naval Research Laboratory, Washington, DC, where his research interests include characterization and performance of microwave-optical devices, microwave fiber-optic links and systems, high-speed optoelectronics, new concepts for solving microwave-related problems with fiber-optic solutions, and high current photodiodes.

Dr. Williams is a member of Tau Beta Pi.

Ronald D. Esman (S'82–M'85–SM'95), for a photograph and biography, see this issue, p. 1278.